

Supplementary Materials

Bis(3-methylthio-1-azulenyl)phenylmethyl Cations and Dications Connected by 1,4-Phenylene Spacer: Synthesis and their Electrochemical Properties

Taku Shoji*, Naoko Sakata, Ryuta Sekiguchi, and Shunji Ito

➤ *Contents*

1. Copies of ^1H NMR, ^{13}C NMR, and COSY of $\mathbf{3a,b}^+\cdot\text{PF}_6^-$ and $\mathbf{4a,b}^{2+}\cdot 2\text{PF}_6^-$ (Figures S1–S12).
2. UV/Vis spectra of $\mathbf{3a,b}^+\cdot\text{PF}_6^-$ and $\mathbf{4a,b}^{2+}\cdot 2\text{PF}_6^-$ (Figures S13–S15).
3. Continuous change in the visible spectra and their photos of $\mathbf{3a,b}^+\cdot\text{PF}_6^-$ and $\mathbf{4a,b}^{2+}\cdot 2\text{PF}_6^-$ (Figures S16–S19).
4. Cyclic voltammograms of $\mathbf{3a,b}^+\cdot\text{PF}_6^-$ and $\mathbf{4a,b}^{2+}\cdot 2\text{PF}_6^-$ (Figures S20–S22).

1. Copies of ^1H NMR, ^{13}C NMR, and COSY of 3a,b $^+$ ·PF $_6^-$ and 4a,b $^{2+}$ ·2PF $_6^-$ (Figures S1–S12).

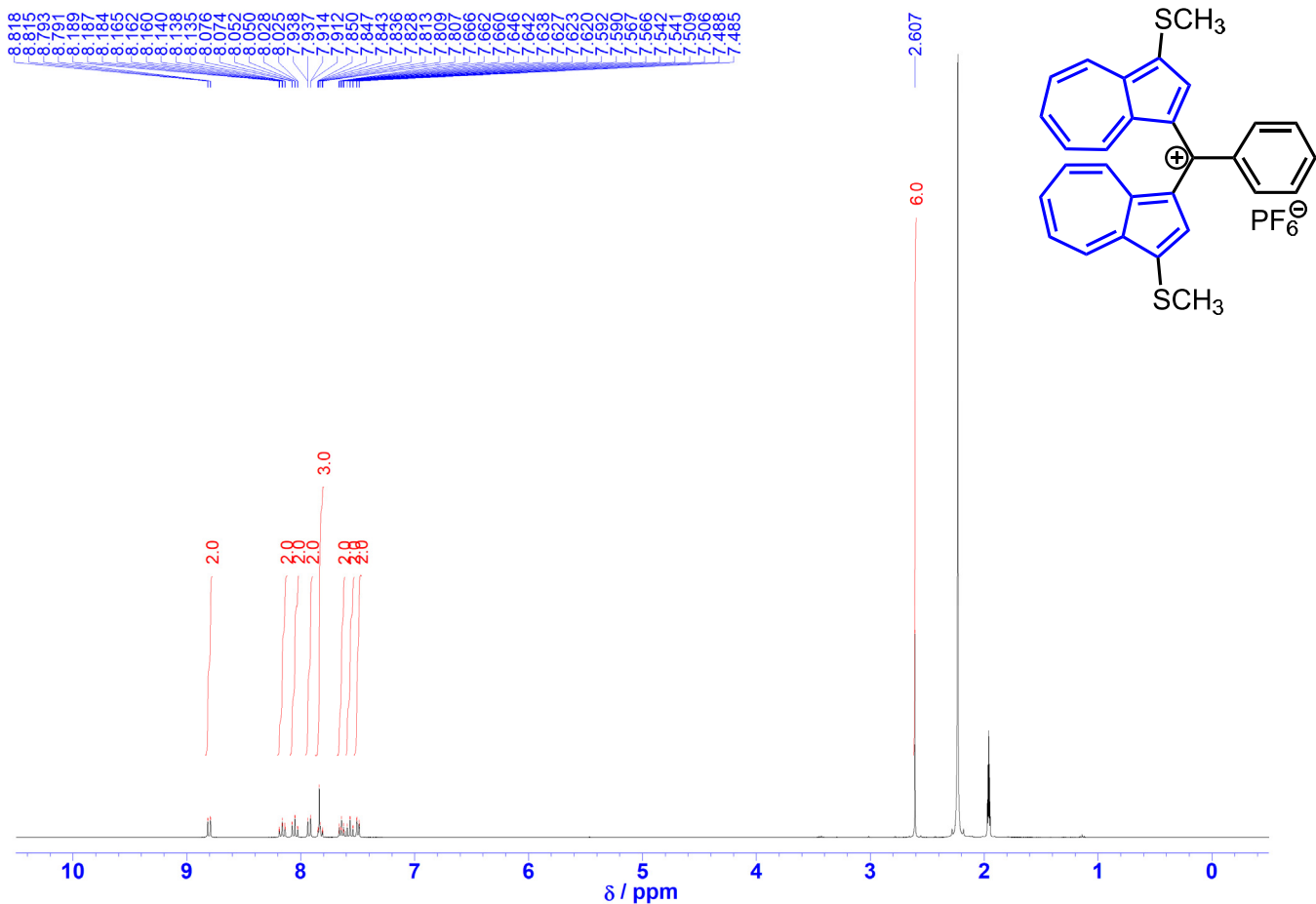


Figure S1. ^1H NMR spectrum of 3a $^+$ ·PF $_6^-$ in CD $_3$ CN (400 MHz).

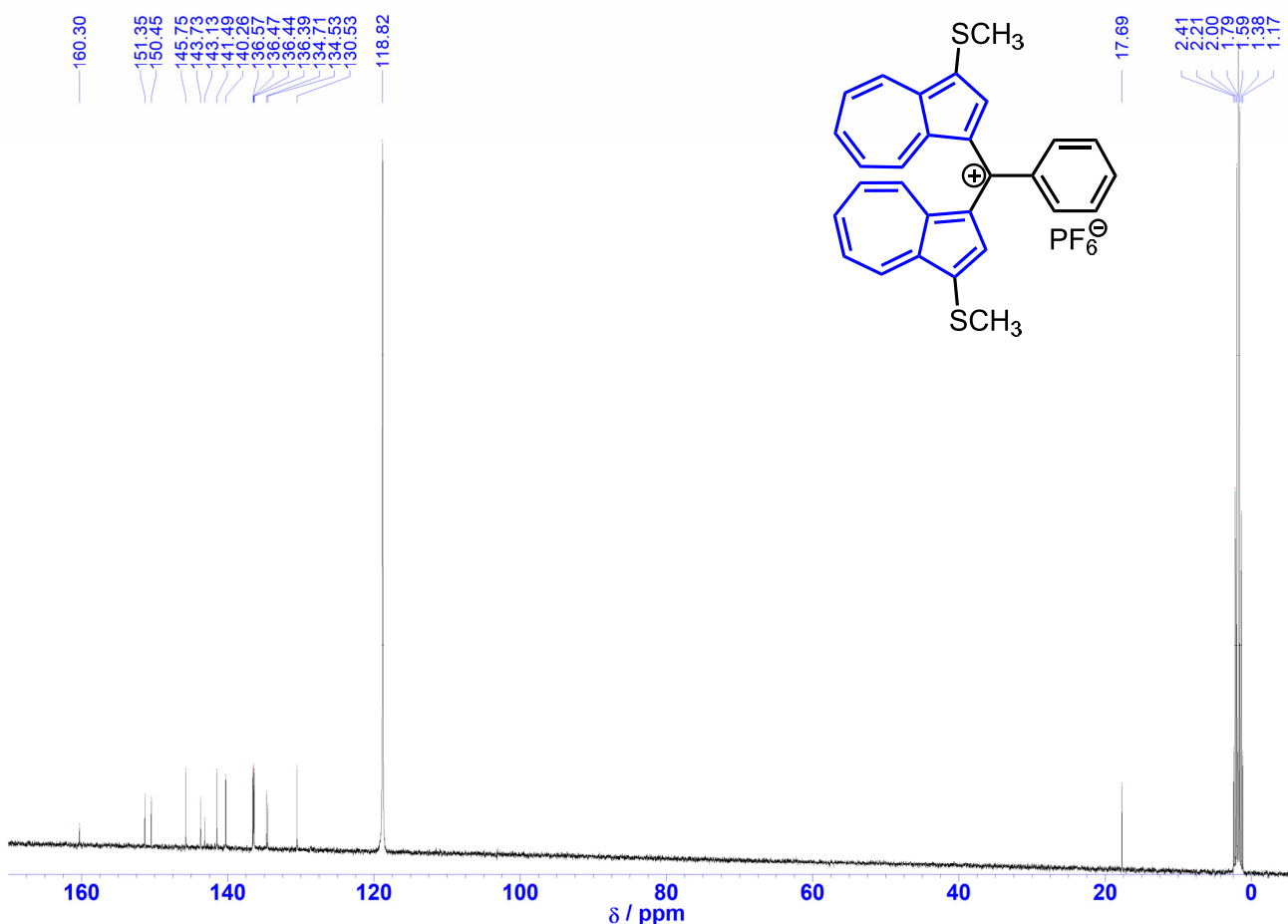


Figure S2. ^{13}C NMR spectrum of 3a $^+$ ·PF $_6^-$ in CD $_3$ CN (100 MHz).

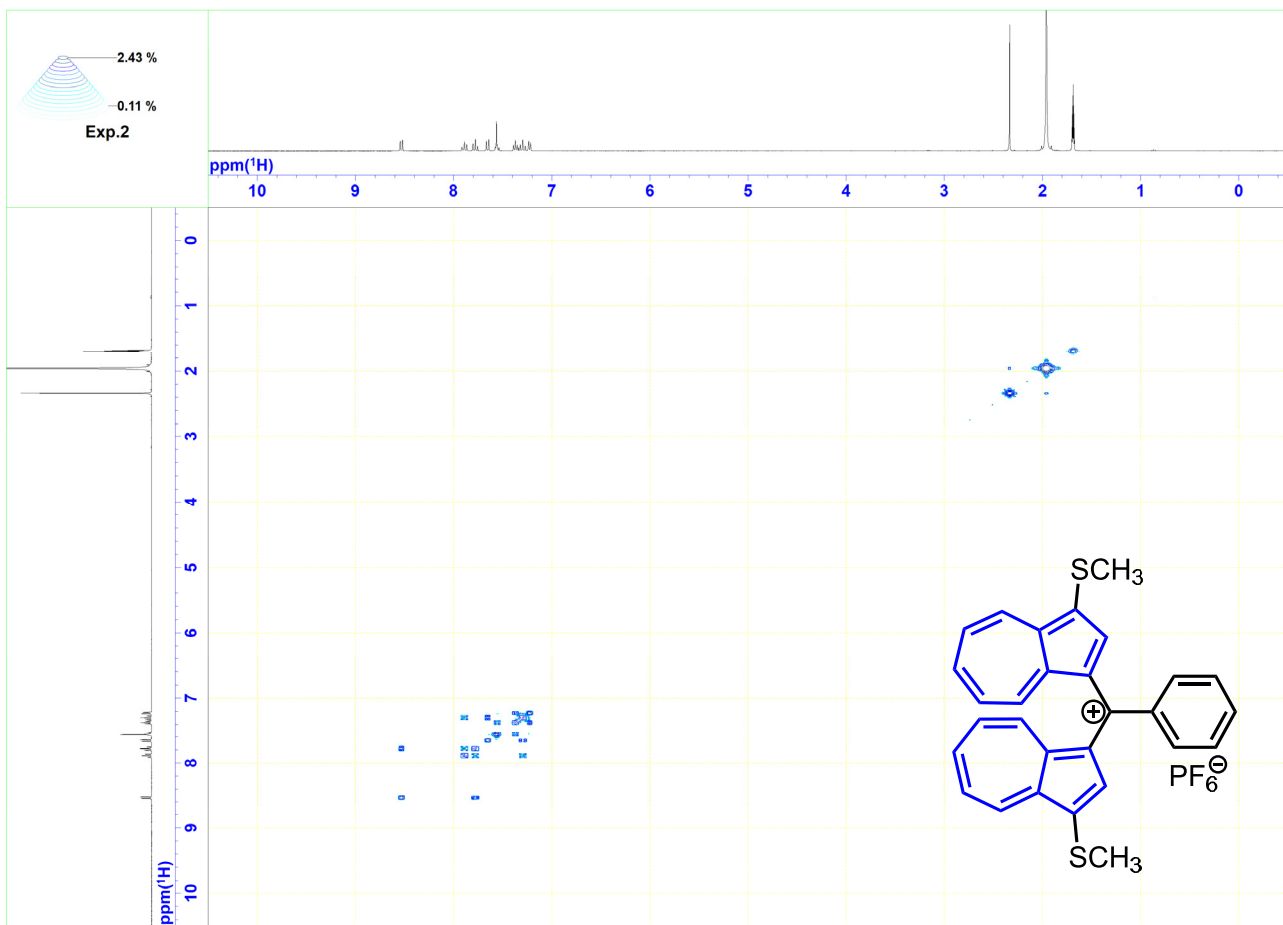


Figure S3. COSY spectrum of $3\mathbf{a}^+\cdot\text{PF}_6^-$ in CD_3CN (400 MHz).

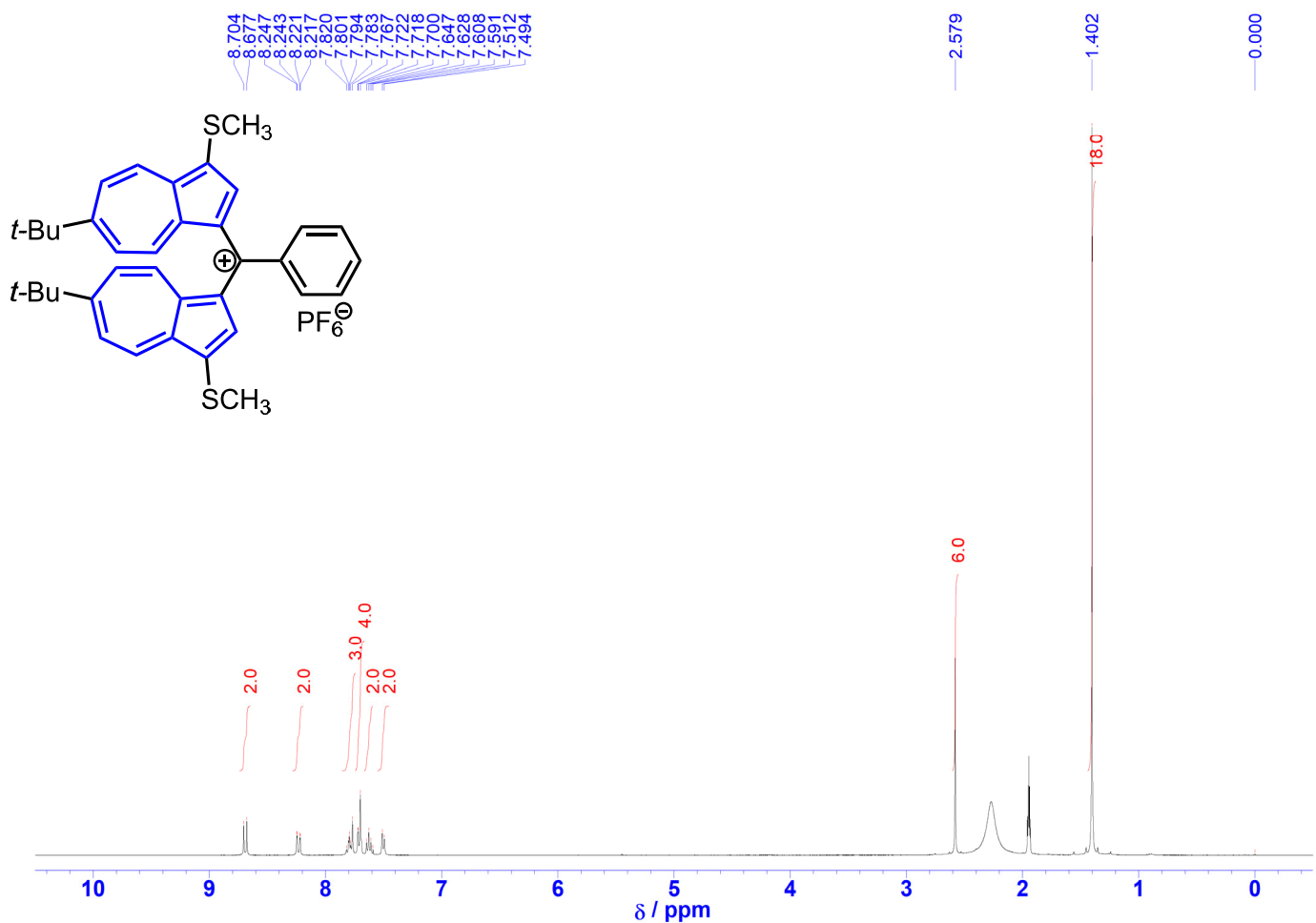


Figure S4. ^1H NMR spectrum of $\mathbf{3b}^+\cdot\text{PF}_6^-$ in CD_3CN (400 MHz).

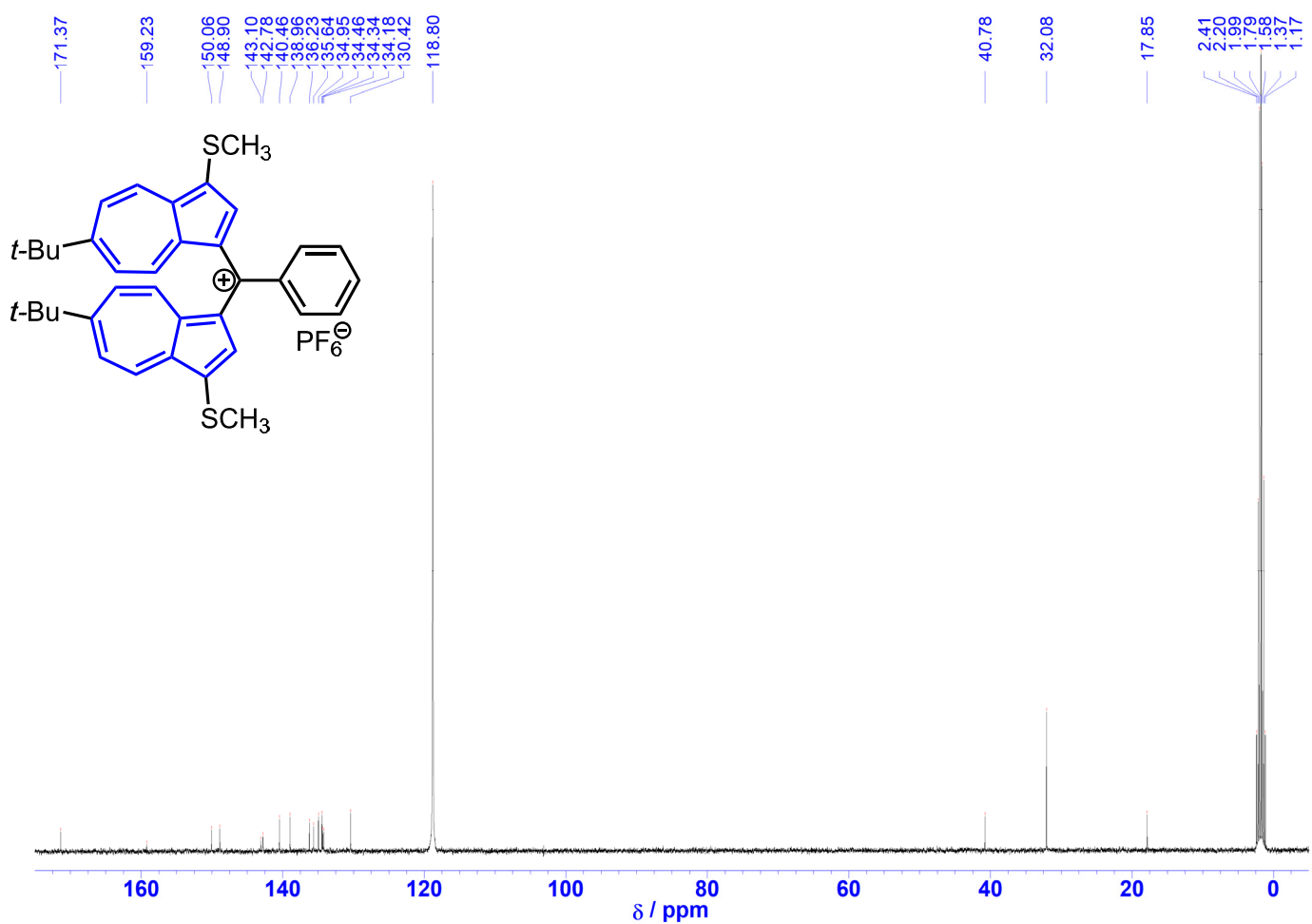


Figure S5. ^{13}C NMR spectrum of $\mathbf{3b}^+\cdot\text{PF}_6^-$ in CD_3CN (100 MHz).

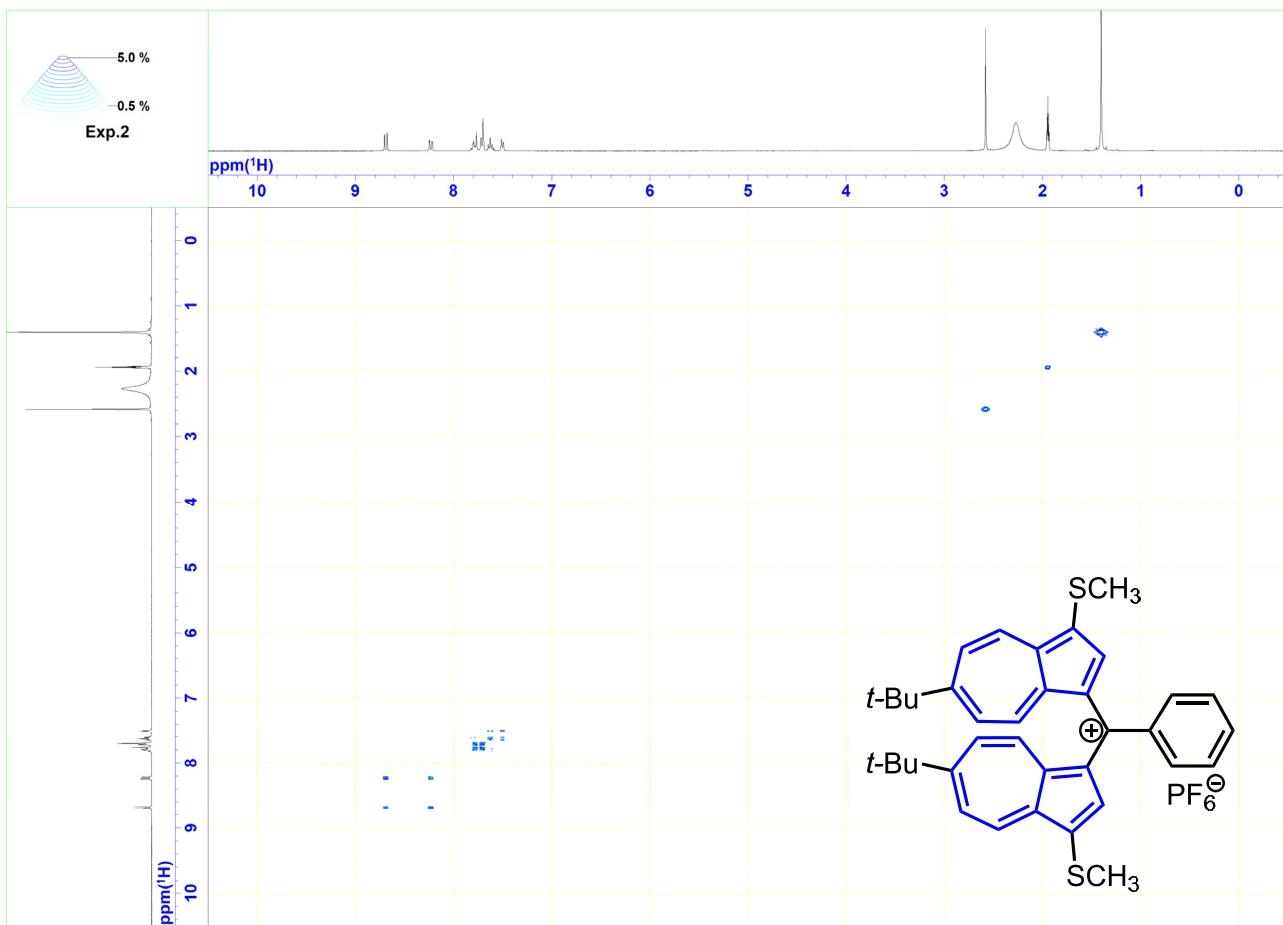


Figure S6. COSY spectrum of $3b^+\cdot PF_6^-$ in CD_3CN (400 MHz).

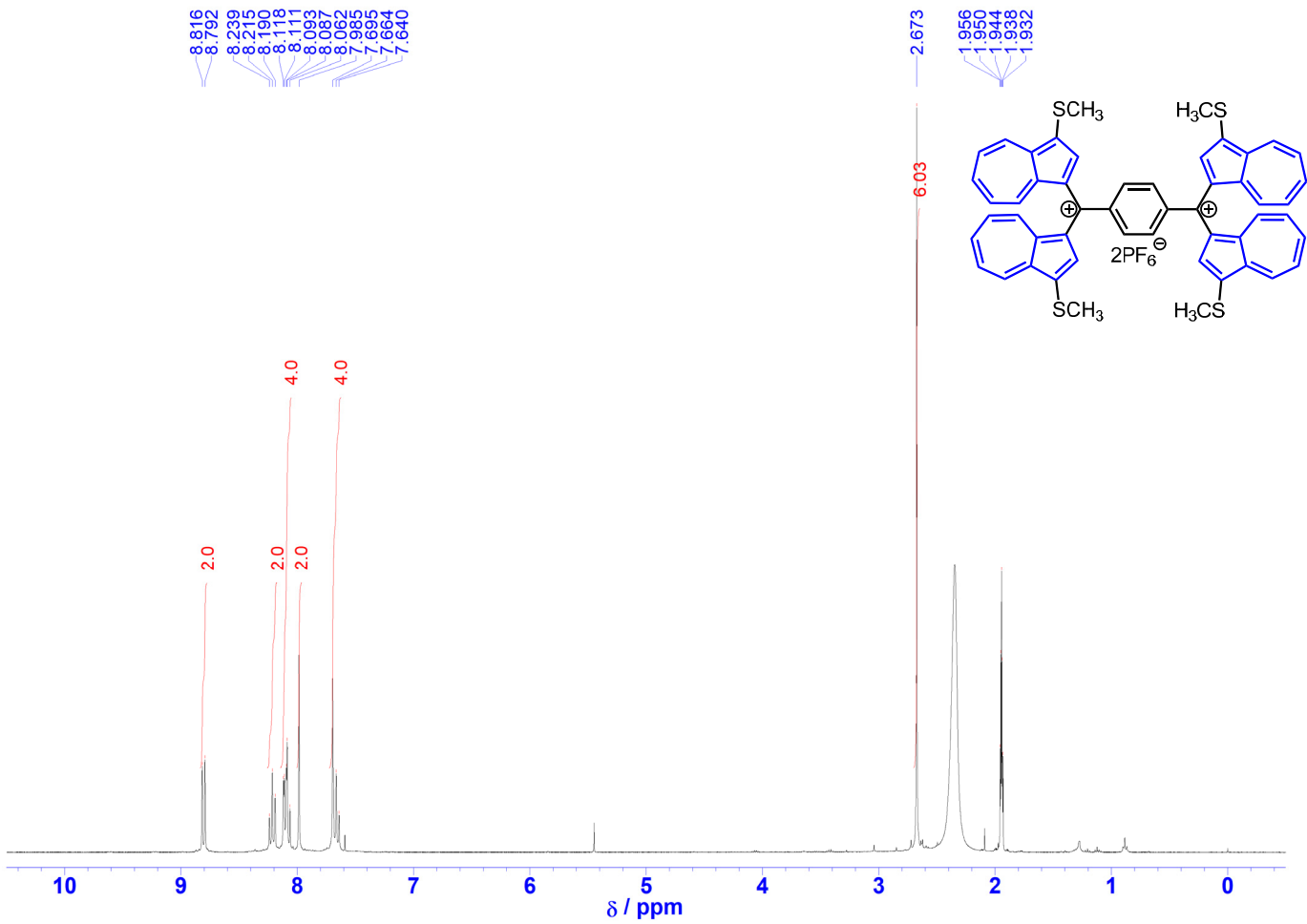


Figure S7. ^1H NMR spectrum of $\textbf{4a}^{2+}\cdot\textbf{2PF}_6^-$ in CD_3CN (400 MHz).

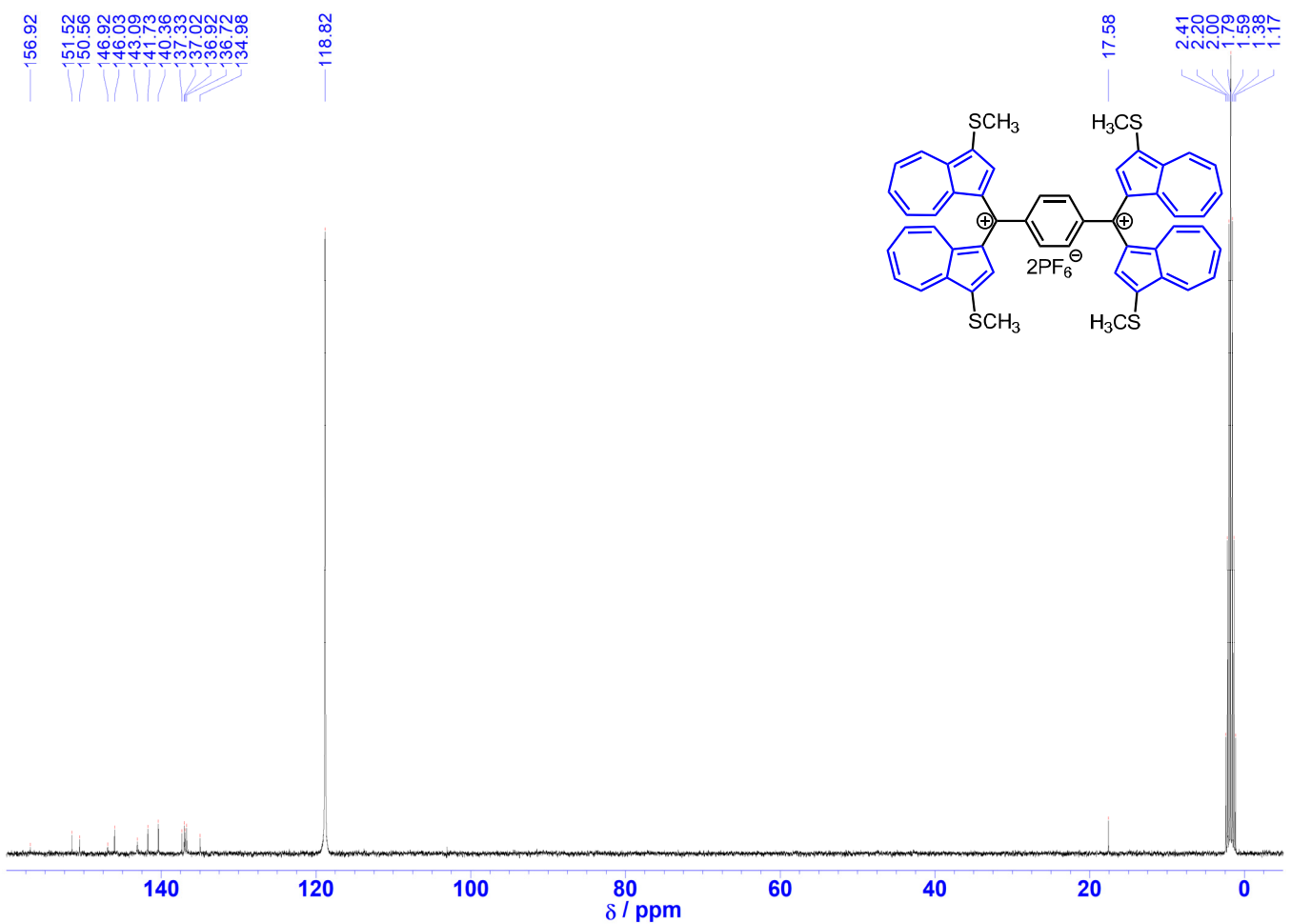


Figure S8. ^{13}C NMR spectrum of $\textbf{4a}^{2+}\cdot\textbf{2PF}_6^-$ in CD_3CN (100 MHz).

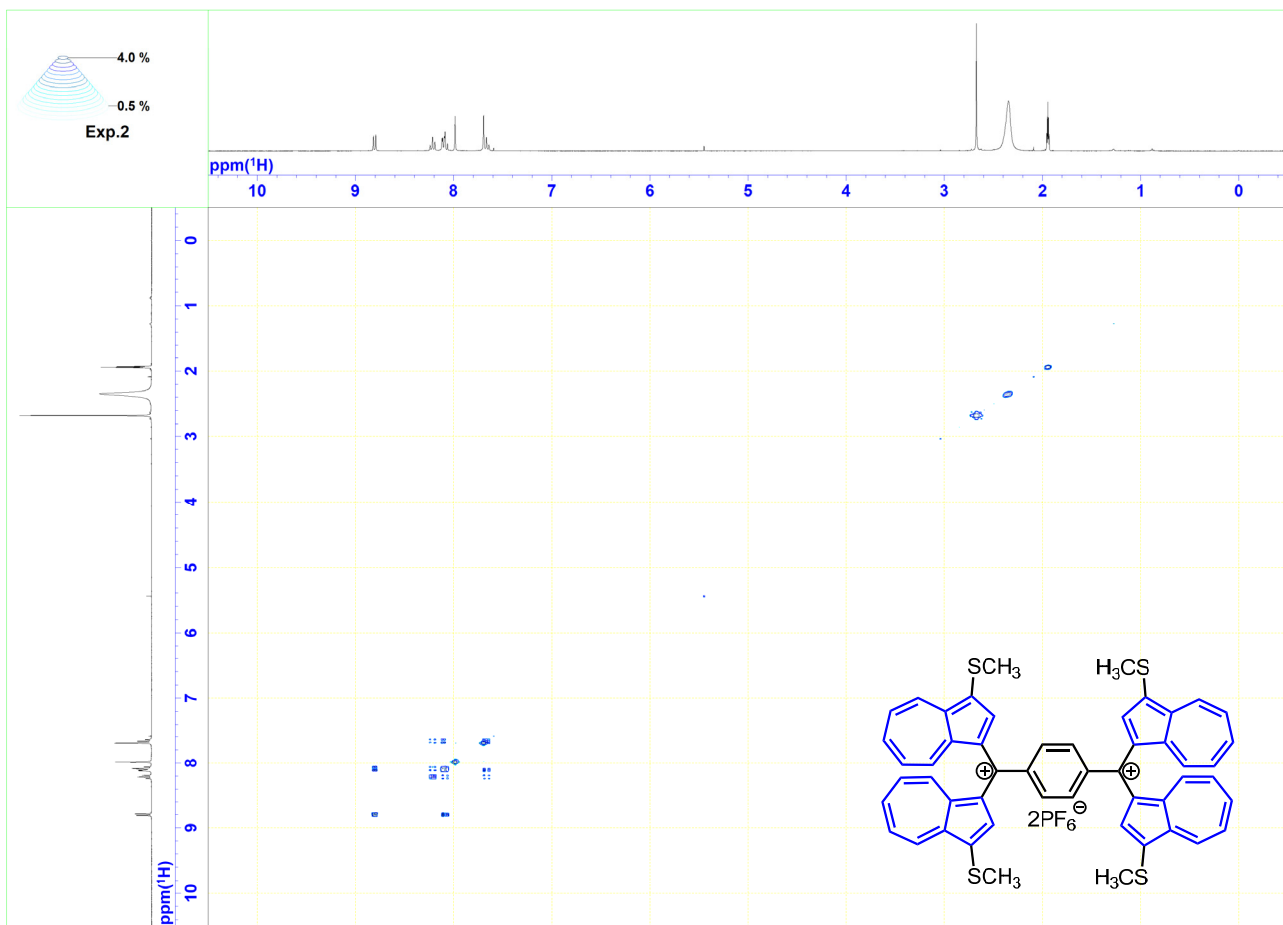


Figure S9. COSY spectrum of $4\text{a}^{2+} \cdot 2\text{PF}_6^-$ in CD_3CN (400 MHz).

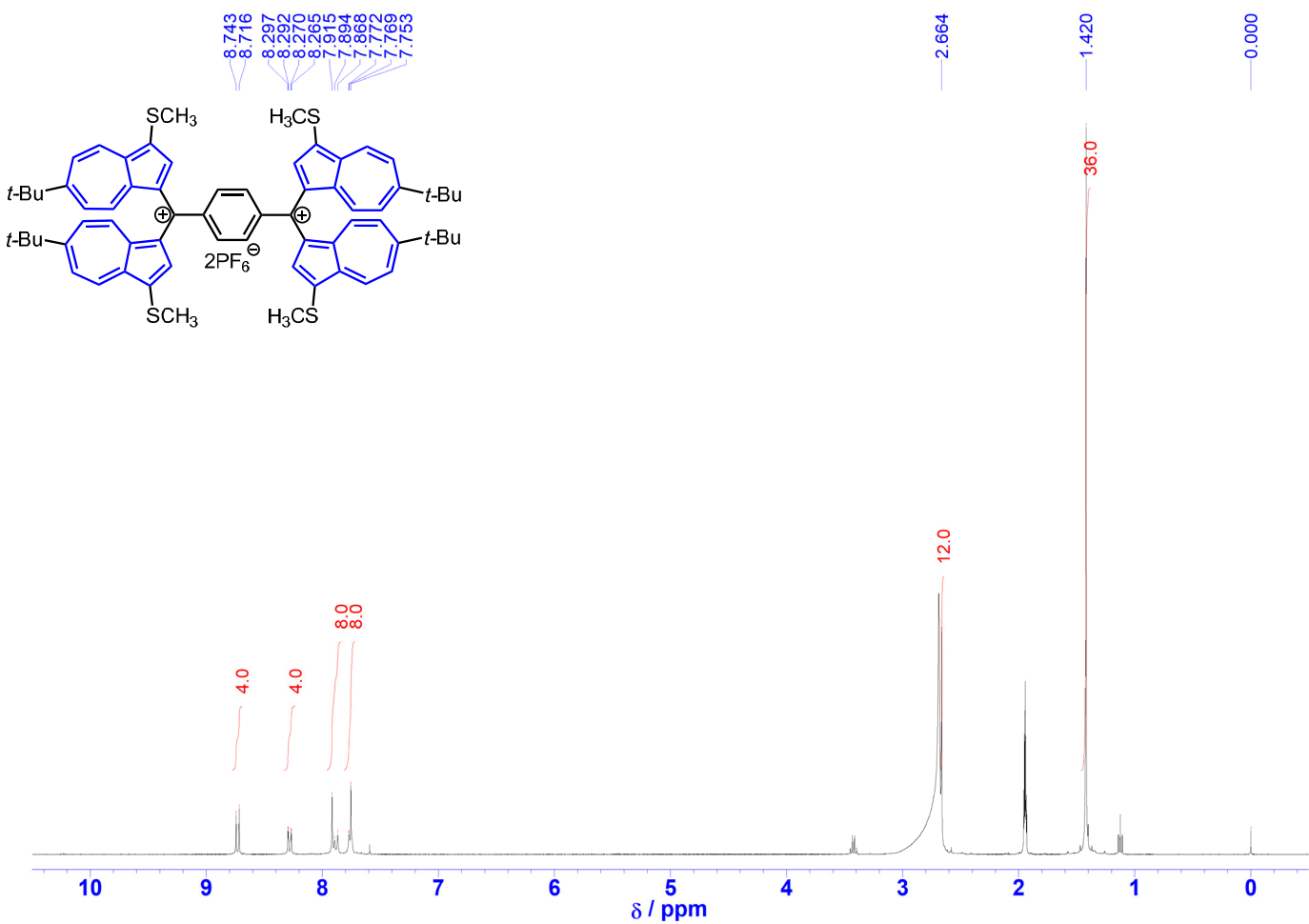


Figure S10. ^1H NMR spectrum of **4b**²⁺·2PF₆⁻ in CD₃CN (400 MHz).

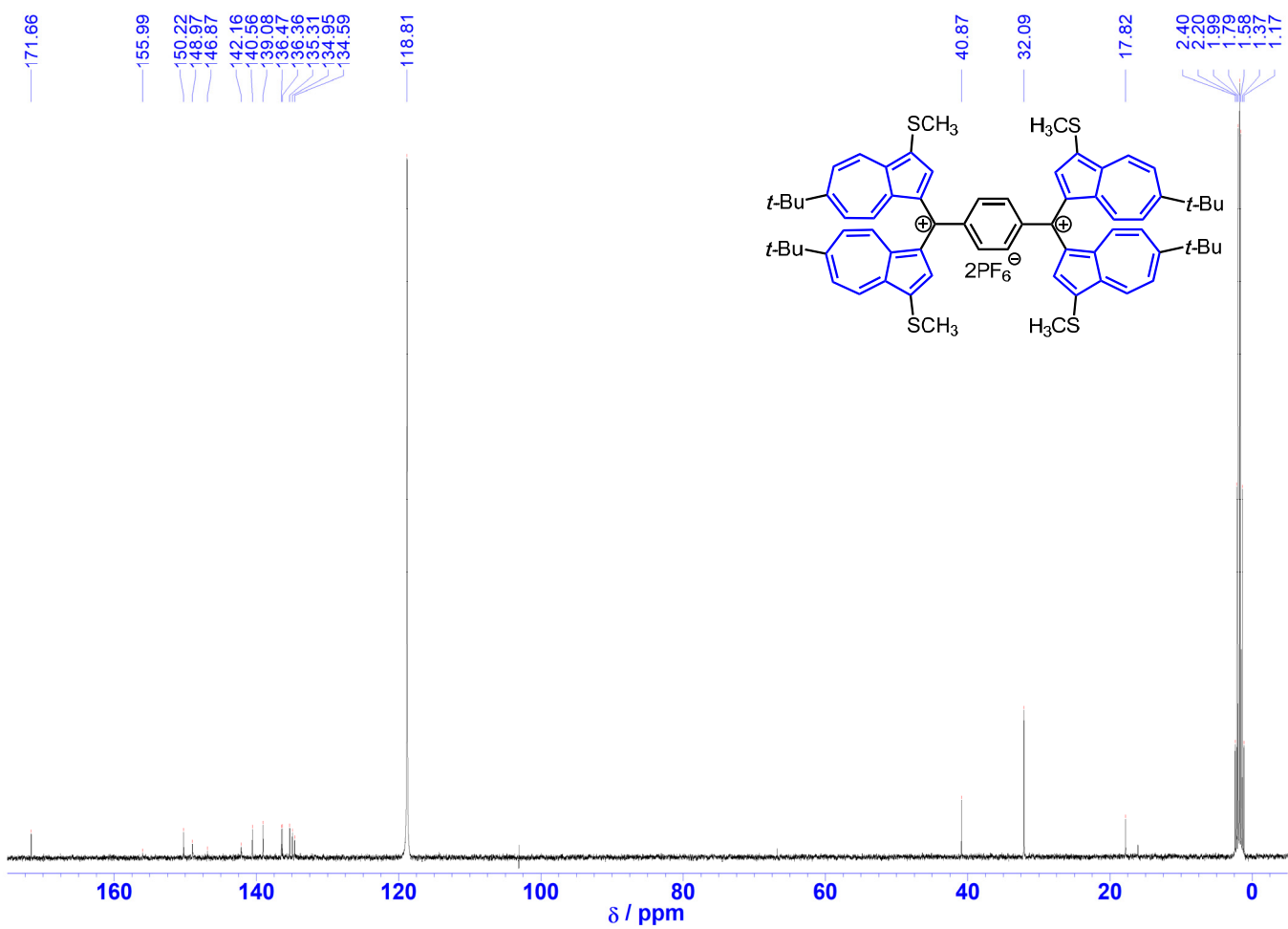


Figure S11. ^{13}C NMR spectrum of **4b**²⁺·2PF₆⁻ in CD₃CN (100 MHz).

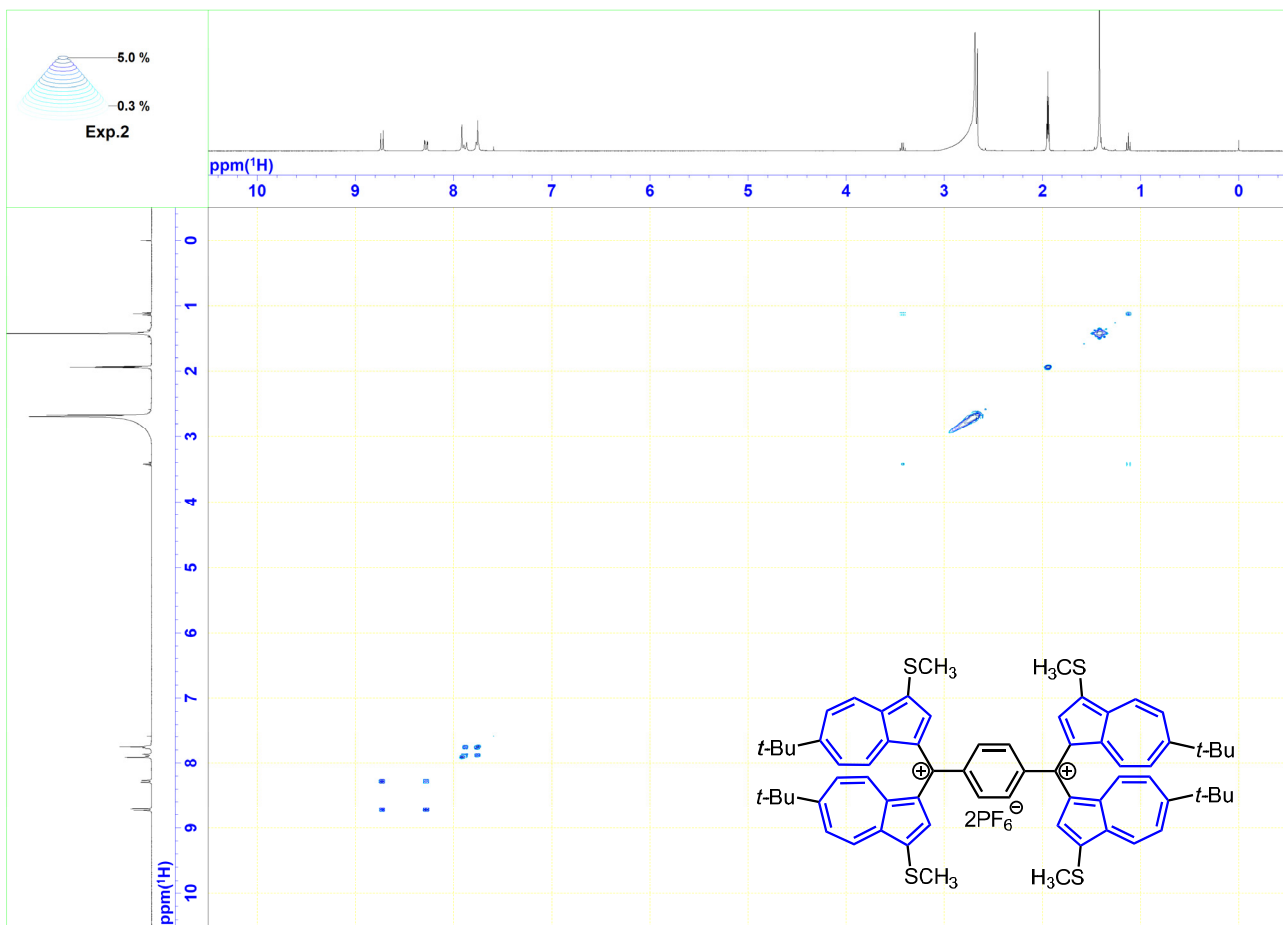


Figure S12. COSY spectrum of $4b^{2+} \cdot 2\text{PF}_6^-$ in CD_3CN (400 MHz).

2. UV/Vis spectra of $3\mathbf{a},\mathbf{b}^+\cdot\mathbf{PF}_6^-$ and $4\mathbf{a},\mathbf{b}^{2+}\cdot\mathbf{2PF}_6^-$ (Figures S13–S15).

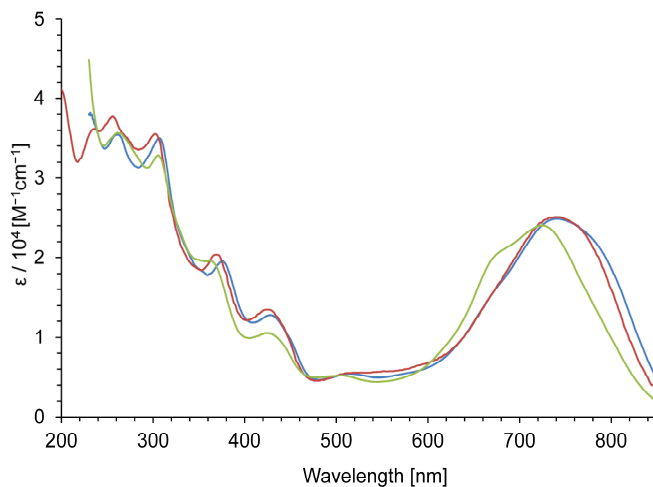


Figure S13. UV/Vis spectrum of $3\mathbf{b}^+\cdot\mathbf{PF}_6^-$ in dichloromethane (blue line), acetonitrile (red line), and hexane (light-green line).

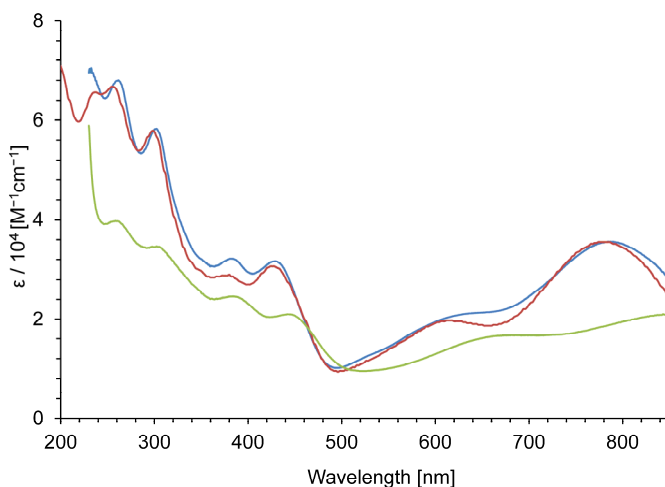


Figure S14. UV/Vis spectrum of $4\mathbf{a}^{2+}\cdot\mathbf{2PF}_6^-$ in dichloromethane (blue line), acetonitrile (red line), and hexane (light-green line).

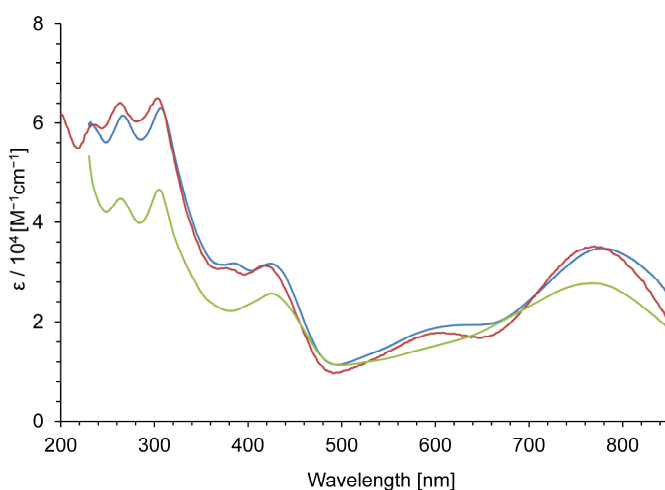


Figure S15. UV/Vis spectrum of $4\mathbf{a}^{2+}\cdot\mathbf{2PF}_6^-$ in dichloromethane (blue line), acetonitrile (red line), and hexane (light-green line).

3. Continuous change in the visible spectra and their photos of $3a,b^+\cdot PF_6^-$ and $4a,b^{2+}\cdot 2PF_6^-$ (Figures S16–S19).

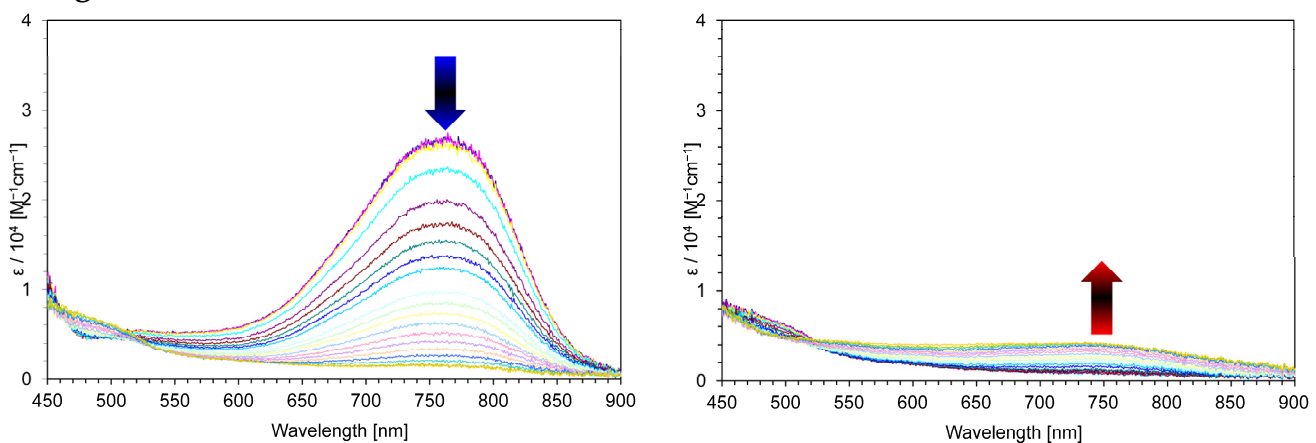


Figure S16. Continuous change in visible spectra of $3b^+\cdot PF_6^-$ in benzonitrile containing Et_4NClO_4 (0.1 M): constant-current electrochemical reduction (50 uA) at 30 sec intervals (left) and the reverse oxidation (right) of the reduced species (50 uA) at 30 sec intervals.



Figure S17. Color changes of $3b^+\cdot PF_6^-$ upon the electrochromic analysis in benzonitrile containing Et_4NClO_4 (0.1 M) upon (50 uA): before electrochemical reduction (left) and after electrochemical reduction (right).

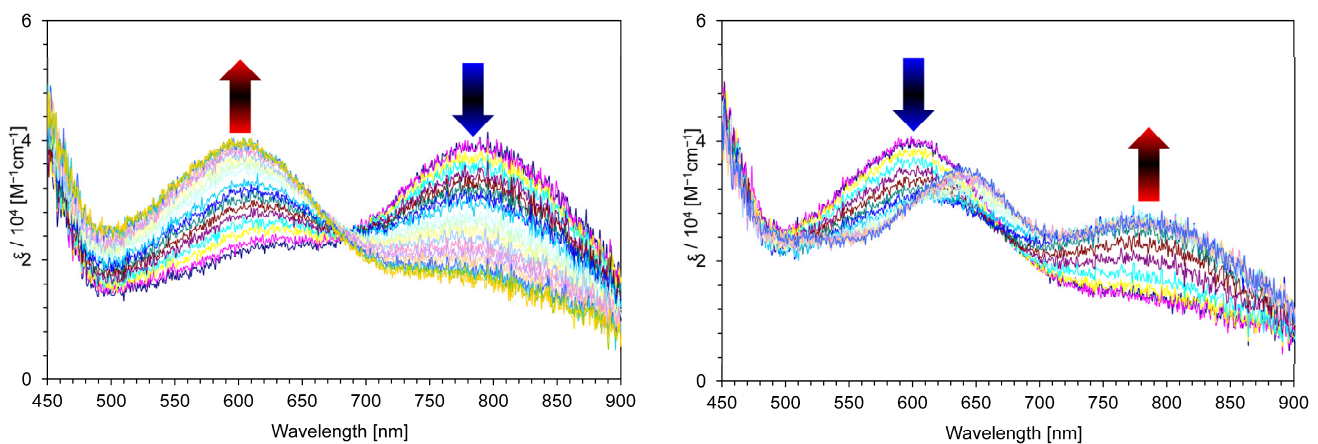


Figure S18. Continuous change in visible spectra of $\mathbf{4a}^{2+}\cdot\mathbf{2PF}_6^-$ in benzonitrile containing Et_4NClO_4 (0.1 M): constant-current electrochemical reduction (50 μA) at 30 sec intervals (left) and the reverse oxidation (right) of the reduced species (50 μA) at 30 sec intervals.



Figure S19. Color changes of $\mathbf{4a}^{2+}\cdot\mathbf{2PF}_6^-$ upon the electrochromic analysis in benzonitrile containing Et_4NClO_4 (0.1 M) upon (50 μA): before electrochemical reduction (left) and after electrochemical reduction (right).

4. Cyclic voltammograms of $3\text{a,b}^+\cdot\text{PF}_6^-$ and $4\text{a,b}^{2+}\cdot2\text{PF}_6^-$ (Figures S20–S22).

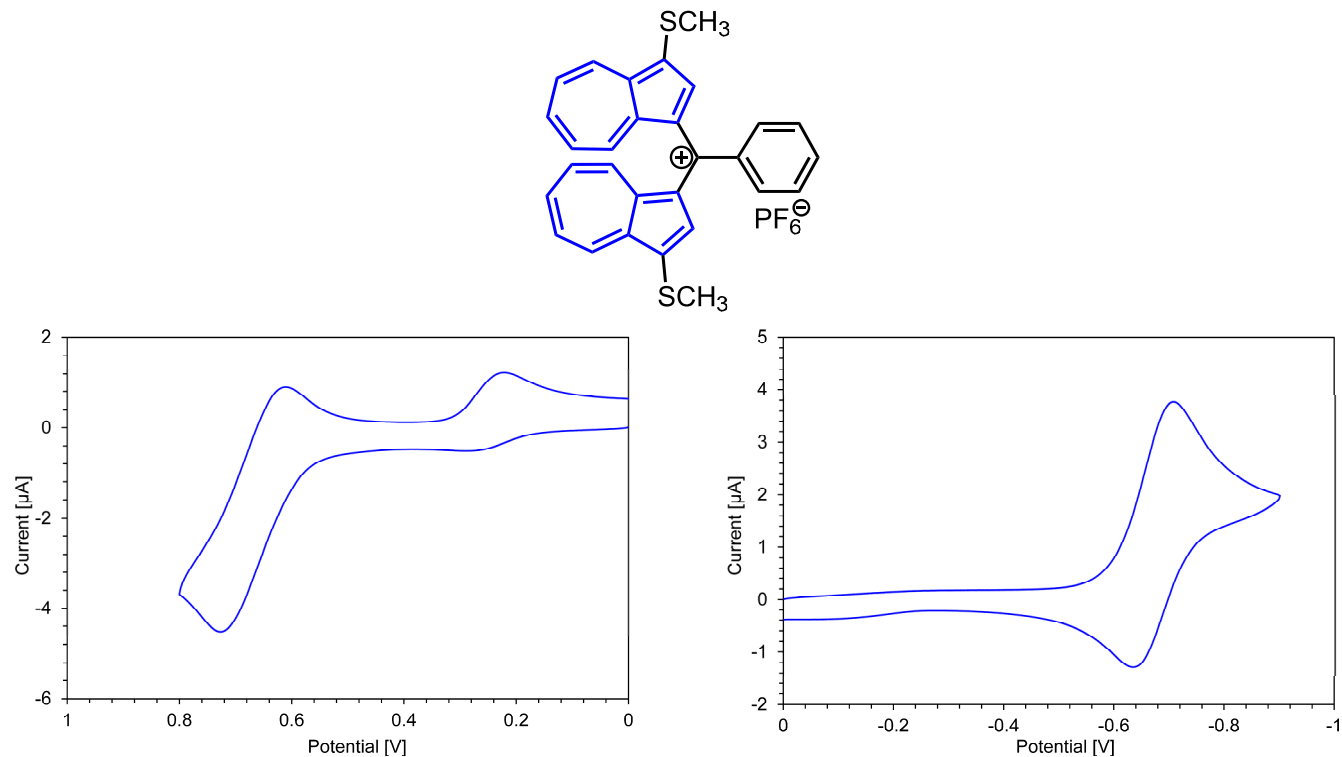


Figure S20. Cyclic voltammogram for oxidation (left) and reduction (right) of $3\text{a}^{2+}\cdot2\text{PF}_6^-$ (1 mM) in benzonitrile containing Et_4NClO_4 (0.1 M) as the supporting electrolyte; scan rate = 100 mVs⁻¹.

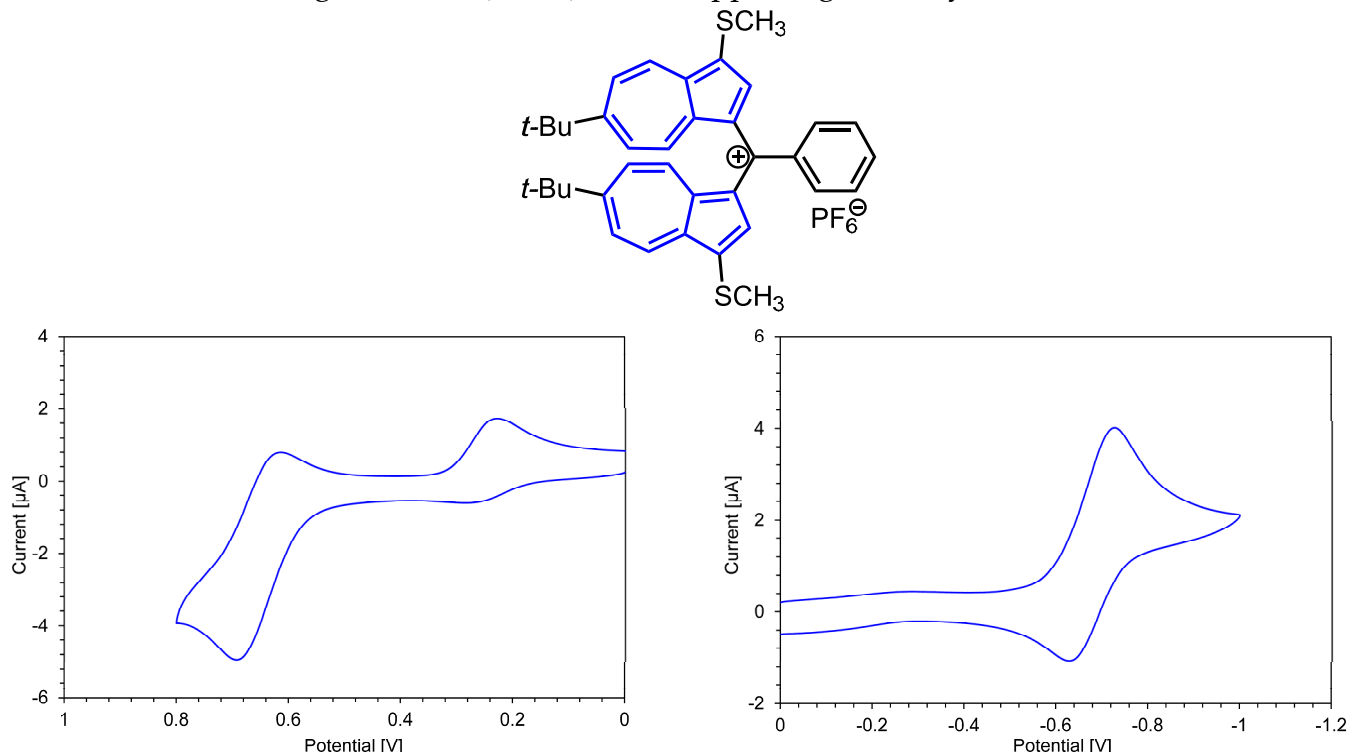


Figure S21. Cyclic voltammogram for oxidation (left) and reduction (right) of $3\text{b}^{2+}\cdot2\text{PF}_6^-$ (1 mM) in benzonitrile containing Et_4NClO_4 (0.1 M) as the supporting electrolyte; scan rate = 100 mVs⁻¹.

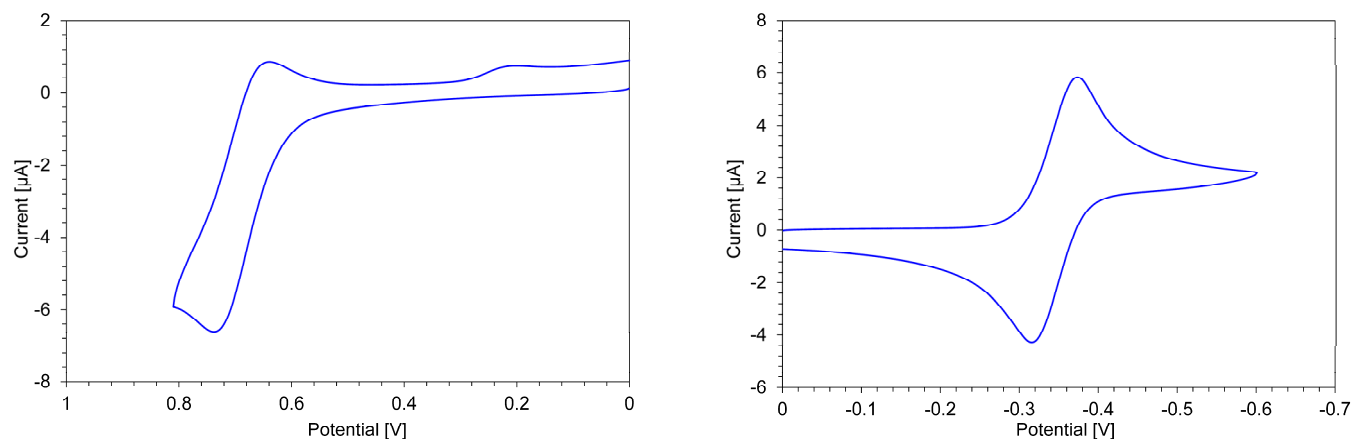
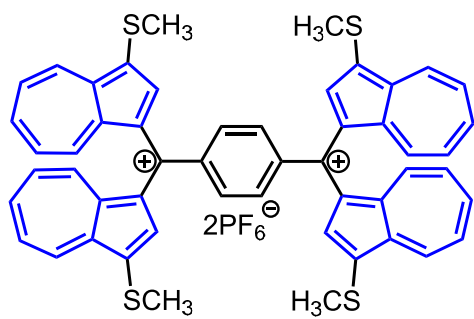


Figure S22. Cyclic voltammogram for oxidation (left) and reduction (right) of $\text{4a}^+\cdot\text{PF}_6^-$ (1 mM) in benzonitrile containing Et_4NClO_4 (0.1 M) as the supporting electrolyte; scan rate = 100 mV s^{-1} .